

Carbon nanotubes: do they toughen brittle matrices?

Johann Cho · Fawad Inam · Mike J. Reece ·
Zdeněk Chlup · Ivo Dlouhy · Milo S. P. Shaffer ·
Aldo R. Boccaccini

Received: 19 December 2010 / Accepted: 10 February 2011 / Published online: 1 March 2011
© Springer Science+Business Media, LLC 2011

Abstract The development of a model CNT-brittle matrix composite system, based on SiO₂ glass containing well-dispersed CNTs at up to 15 wt%, allows a direct assessment of the effect of the nanoscale filler on fracture toughness (K_{IC}). Samples were prepared by colloidal heterocoagulation followed by spark plasma sintering. Detailed K_{IC} measurements, using both indentation and notched beam techniques, show a linear improvement with CNT content, with up to a twofold increase of fracture toughness at maximum loading. The results from the two methods used in this study show equivalent trends but differing absolute values; the relative merits of these two approaches to measuring nanocomposite toughness are compared. Possible toughening mechanisms associated with CNT pull-out, crack bridging, and crack deflection are

identified, and discussed quantitatively, drawing on conventional short-fibre composite theory and the potential effects of scaling fibre diameter.

Introduction

Carbon nanotubes (CNTs) are considered to have excellent potential as reinforcements in a wide range of composite systems, due to their exciting intrinsic mechanical and other functional properties [1–4]. The vast majority of CNT composite work has focussed on polymer matrices, whilst comparatively few investigations have explored inorganic (ceramic and glass) matrices [5]. However, in the last decade, there has been growing interest in using CNTs in brittle ceramic monoliths, particularly as toughening agents in these otherwise strong and stiff materials [6–14]. Whilst CNTs are sometimes viewed as a ‘new generation’ of carbon fibre, the mechanical effects of a thousand-fold diameter reduction, to a length scale that is closer to molecular dimensions than conventional fibres, is not yet clear. In addition to any improvements in toughness, CNTs may have a significant influence on other properties such as electrical conductivity, thermal expansion coefficient, hardness, and thermal shock resistance. CNTs have also been reported to improve the sinterability of ceramic nanocomposites [15]. The combination of these properties with the intrinsic advantages of ceramic materials such as high temperature stability, high corrosion resistance, and light weight makes CNT/ceramic composites very attractive functional and structural materials for a variety of applications. A recent comprehensive review [5] discusses the various processing routes developed in order to explore the use of CNTs in ceramic matrix composites, and summarises the resulting properties.

J. Cho · A. R. Boccaccini
Department of Materials, Imperial College London,
London SW7 2AZ, UK

J. Cho · M. S. P. Shaffer (✉)
Department of Chemistry, Imperial College London,
London SW7 2AZ, UK
e-mail: m.shaffer@imperial.ac.uk

F. Inam · M. J. Reece
Nanoforce Technology Ltd and School of Engineering
and Materials Science, Queen Mary University of London,
London E1 4NS, UK

Z. Chlup · I. Dlouhy
Institute of Physics of Materials, ASCR, 61662 Brno,
Czech Republic

A. R. Boccaccini (✉)
Department of Materials Science and Engineering,
University of Erlangen-Nuremberg, 91058 Erlangen, Germany
e-mail: aldo.boccaccini@ww.uni-erlangen.de

Although CNTs have been reported to toughen brittle matrices in a number of studies [5–14], the quantitative extent of the effect is still unclear. In many cases, due to the limited supply of materials and unusual processing challenges, only a small number of samples have been tested, at a small range of relatively low loading fractions, often using non-standard methods. In most cases, it is difficult to isolate the influence of the CNTs on composite fracture toughness from changes in the matrix microstructure; the incorporation of CNTs can influence, for example, grain size, grain orientation, and overall crystallinity. The state of CNT dispersion, which is very difficult to quantify, is sometimes not even described, despite the potential significance of agglomerates or segregation to grain boundaries. Whilst different toughening mechanisms have been qualitatively suggested by considering the appearance of the fracture surface, there is surprisingly little discussion of their quantitative contribution.

The different results reported in literature have led to a continuing debate [7–11] on the appropriateness of different fracture toughness measurement methods (IF: indentation fracture toughness, SENB: single edge notch beam fracture toughness) as applied to CNT/ceramic matrix composites. The problem of identifying the actual toughening effect of CNTs is particularly acute in polycrystalline ceramics [6, 7], where variations in matrix microstructure obscure the ‘true’ toughening effect of CNTs. Similar problems are encountered with glass–ceramics [13], as the majority of studies do not consider changes in the degree of crystallinity, crystallite size or orientation in the glassy matrix that are likely to be induced by the presence of CNTs.

For these reasons, the present investigation focuses on introducing CNTs into glass matrix composites; the result is a model system in which microstructural variations associated with grain size, orientation, and boundaries are avoided by providing an amorphous linear elastic matrix. Fully dense CNT/silica glass matrix composites were produced by Spark Plasma Sintering (SPS) of heterocoagulated powder of CNTs and colloidal SiO₂ nanoparticles. The resulting composites were subjected to both indentation fracture and chevron notch fracture toughness measurements, providing a direct comparison of both methods on reproducible, model, CNT-containing composites.

Experimental

Carbon nanotubes

Multi-walled carbon nanotubes (CNTs) used in this study were synthesised by the injection catalytic chemical vapour deposition (CCVD) method, in which metallocene

(ferrocene) dissolved hydrocarbon solution (toluene) was injected in an inert gas flow. Details of the method are given elsewhere [16]. As-synthesised CNTs were refluxed in concentrated H₂SO₄/HNO₃ (3:1 volume ratio) mixture at 120 °C for 30 min to purify and improve the surface chemistry of CNTs. Once oxidised, the CNTs were then thoroughly washed with distilled water on 0.2 µm pore PTFE membrane, until the filtrate was colourless and showed no acidity. The CNT/H₂O suspension was sonicated in ultrasonic bath, and centrifuged at 3000 rpm for 15 min to remove any remaining aggregates. The as-refluxed CNT solution was diluted to 0.5 mg/mL, then diluted further by mixing with ethanol (H₂O:EtOH = 1:1 by volume). The final concentration of CNT in the (H₂O+EtOH) solvent was 0.25 mg/mL and the average oxidised nanotube length was $L \approx 4.2 \mu\text{m}$

CNT/SiO₂ composite fabrication

The as-prepared CNT suspension was added drop-wise (400 mL/h) using a peristaltic pump to an equal volume of magnetically stirred (300 rpm) silica suspension (RH200S, Degussa, Germany) to promote electrostatic attraction between the two phases. The heterocoagulated suspension was dried in a standard oven at 80 °C to extract the solvent mixture, and calcined at 350 °C for 3 h in air to burn out any possible remaining organic residues. The powder mixture was compacted using a uniaxial press in a 30 mm graphite die prior to sintering. SPS was used to densify the materials to avoid degradation of the CNTs during processing [17]. The pre-compacted mixture was first heated to in a vacuum (5 Pa) to 450 °C using a heating rate of 100 °C/min and uniaxial pressure of 5 MPa, and then to the target temperature of 1200 °C at a heating rate of 100 °C/min, under a linearly increasing uniaxial pressure, reaching 75 MPa at the target temperature. The pressure and temperature were then maintained for 20 min, before releasing the pressure and cooling to room temperature at 100 °C/min. Composites were prepared containing up to 15 wt% CNTs.

Characterisation methods

Scanning electron microscopy

Field emission gun-scanning electron microscopy (FEG-SEM, 5 kV, Leo Gemini, Carl Zeiss, Hertfordshire, U.K.) was used to observe polished and fractured surfaces of selected samples. Sintered samples with low CNT loadings (<5 wt%) were sputter-coated prior to SEM, but other samples with high CNT contents were observed as-produced. SEM micrographs were used also to quantify the length and diameter of the nanotubes in the initial

dispersions. A total of 150 nanotubes per each sample were examined by using image analysis software (ImageJ, NIST, US). The average length and diameter of the various carbon nanotube samples are reported with their standard deviations.

XRD

A Philips X-ray diffractometer (PW2273/20) was used to identify possible crystalline phases in sintered composite samples. Cu K α radiation was used in the 2θ range from 10° to 55° with a step size of 0.02° , integrated for one second per step.

Vickers indentation fracture toughness (IF)

A computer-controlled microhardness tester (Zwick/Roell Indentec ZHV, at 1 kg for 10 s) was used for determination of microhardness and indentation fracture toughness. At least 10 measurements were carried out on each sample, in well-separated, randomly selected regions. A larger number of indentation tests were carried out during preliminary tests but offered no significant improvement in the scatter of data; therefore, indentation cracks and toughness values from 10 independent indentations were considered sufficient for this study. The equation derived by Anstis et al. [18] and verified for glass matrix composite systems elsewhere [19] was used to calculate the indentation fracture toughness (K_{IC} , MPa m $^{-1/2}$):

$$K_{IC} = 0.0154 \times \left(\frac{E}{H}\right)^{1/2} \cdot \left(\frac{P}{C^3/2}\right) \quad (1)$$

where E is Young's modulus, H is hardness, P is load, and C is average radial crack length. To apply the equation, experimental Vickers hardness and elastic modulus (determined by Grindosonic) values were determined at each CNT concentration. E/H values, however, did not change much with CNT content ($E/H \sim 17$).

Chevron notch beam fracture toughness (CNF)

Rectangular bar samples ($2 \times 3 \times 25$ mm) were prepared with chevron notches cut using a thin diamond wheel saw (thickness = 0.2 mm). The crosshead speed during 3-point bending testing was 0.01 mm/min and the load cell capacity was 1 kN. At least five samples were tested for each condition. Graphs of load versus deflection were recorded and the fracture toughness calculated from the maximum load (F_{max}) and the corresponding minimum value of geometrical compliance function (Y_{min}^*) using the following equation [20]:

$$K_{IC} = \frac{F_{max}}{BH^{1/2}} \times Y_{min}^* \quad (2)$$

where B and H are the breadth and height of the specimens, respectively.

Results

Microstructural analysis

The relative density of the sintered samples was measured by Archimedes' method and found to exceed 98% in all cases, independently of CNT content. An intrinsic CNT density of 1.65 g cm $^{-3}$ was used, based on linear extrapolation of the density/loading fraction data; the value is typical of MWNTs [2]. SEM observations of fracture surfaces (Fig. 1) confirmed the almost total absence of porosity and that the excellent nanotube distribution found in the green body was maintained following the high temperature consolidation process. There are no obvious alignment effects; indeed, the uniaxial process is expected to lead to approximately random CNT orientation with only a weak in-plane tendency. Extensive pull-out, as seen in Fig. 1b, is helpful for imaging the distribution of CNTs; the implications for toughening are discussed in detail below. The maximum and average CNT pull-out lengths were determined to be: 1.2 μ m and 700 ± 200 nm (average of 100 independent nanotubes measured from SEM images), respectively, for the 15 wt% composite.

XRD patterns (Fig. 2) show two small characteristic peaks at $2\theta=22^\circ$ and 27° , attributed to cristobalite and CNTs (graphite), respectively, over a broad amorphous silica background. The analyses show that no other crystalline phases (as a result of possible reaction between CNTs and the silica matrix) have formed during the sintering processing. The cristobalite peak is weak when compared to the XRD spectrum of fully crystallised silica monoliths (inset in Fig. 2); the degree of crystallinity can be estimated by normalising the area under the peak intensity at $2\theta=22^\circ$ with the area of background spectrum obtained on amorphous samples. Even the 1 wt% CNT composite sample, which has the largest area under the peak, has an estimated crystallinity of less than 5%; the composites with higher nanotube content display a monotonically decreasing degree of crystallinity and can be considered to have an essentially amorphous matrix. Despite the potential nucleating effect of a heterogenous surface, the presence of CNTs appears to suppress the crystallisation of silica. This effect may be associated with reduced mobility of the silica network bound to the nanotube surface, or to the local stiffness of the nanotubes

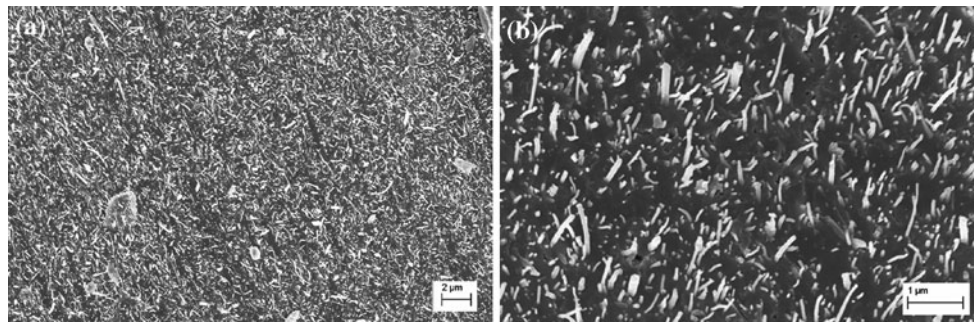
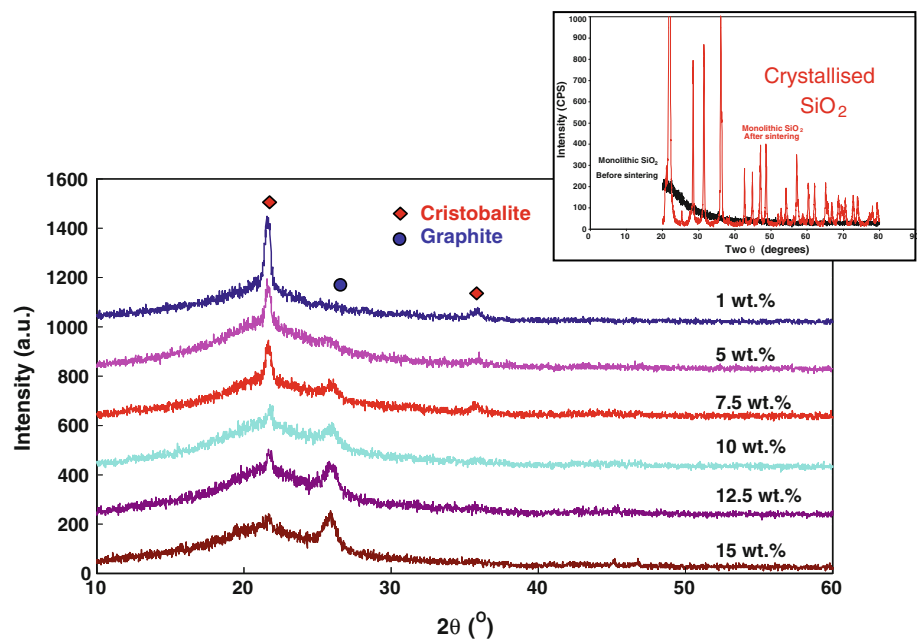


Fig. 1 SEM images showing fracture surfaces of sintered 15 wt% CNT/silica composites at **a** low, and at **b** high magnification

Fig. 2 XRD spectra confirming that sintered composite samples have the minimal cristobalite crystallisation. *The inset shows the XRD spectrum of the fully crystallised silica monolith (no CNTs)*



opposing the volume reduction associated with crystallisation. Further analysis is beyond the scope of this study, although we have observed identical behaviour for samples consolidated by pressureless sintering, in several independent studies (unpublished data). Importantly, the low level of crystallinity is unlikely to have a significant influence on the properties. If there were any reinforcing effect of the crystallites, it would decline with increasing CNT content, so could not lead to an overestimation of the CNT contribution.

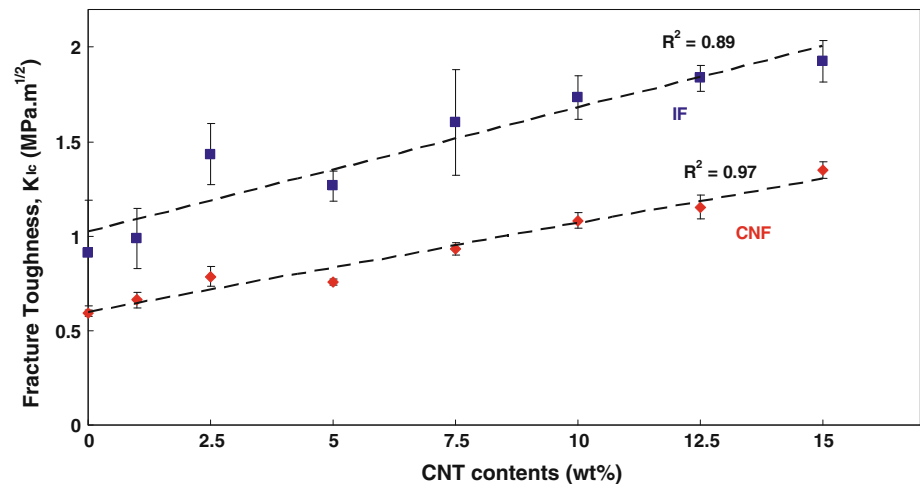
Fracture toughness measurements

The fracture toughness values measured by both indentation fracture (IF) and chevron notch fracture (CNF) tests are compared in Fig. 3. Both methods show similar trends, with a roughly linear increase in toughness. The absolute values of K_{IC} measured by the two techniques differ, but the relative improvement over the matrix value is very

similar, reaching around 120% improvement for the 15 wt% composites. Both methods show a slight sub-linear deviation for the 5 wt% sample, suggesting a systematic issue with this material, but highlighting the similar sensitivity of the two approaches. IF data (not shown) were obtained for cracks running perpendicular and parallel to the uniaxial pressing direction, but no difference was observed within error, confirming the lack of significant orientation effects in the current context.

Although all fracture toughness measurement methods have some drawbacks, the validity of the IF technique to determine K_{IC} of CNT–ceramic composites has been specifically questioned in the literature [8, 21]. In the indentation test, the size of the cracks formed depends on the nature of the elastic–plastic damage response of the relatively small volume of material under the indenter. Therefore, some caution must be exercised before making quantitative claims about the absolute magnitude of fracture toughness. Wang et al. [7] suggested that CNT

Fig. 3 Fracture toughness results measured by indentation fracture (IF) and chevron notch fracture (CVF) test methods, as a function of CNT content



additions may allow shear deformation under the indenter, which limits the cracking (shorter cracks or even no cracking) around the indentation, resulting in artificially high fracture toughness values. In this study, the classical radial cracks at the corners of the indented region were observed for both monoliths and composite samples (with shorter crack lengths found for the composite samples). The parallel trends in the IF and CNF data suggest that localised shear deformation did not significantly affect the IF results, although the IF data does show larger scatter, as indicated by the error bars in Fig. 3. As expected, the discrepancy between the two data sets is greater than the experimental error and reflects fundamental differences in loading geometry, stress state, measurement technique, and sample preparation. Given the systematic offset between the two methods, it seems clear that the indentation technique should not be used to determine absolute values of K_{IC} in CNT/ceramic composites [5]; however, despite the criticism in the literature, the data demonstrate that IF can be used to rank CNT composites effectively, for well-densified materials with a good nanoscale dispersion. The IF test remains attractive for its simplicity and minimal material demands; as well as indicating relative fracture toughness, it can be used to assess contact damage resistance and hardness.

Figure 4 compares known literature data for CNT–inorganic matrix composites to the new fracture toughness results shown in Fig. 3. The plot highlights the unusually high loading fractions that have been successfully processed in this study to yield a linear response. Other than the labelled data points, mostly associated with the indicated microstructural variations [6, 7, 13, 22, 23], the scatter of data masks any systematic variation between the Vickers and SENB data, again suggesting that both methods provide a reasonable measure of relative improvements. The K_{IC} improvement obtained in the current study is consistent but relatively modest. However, the more

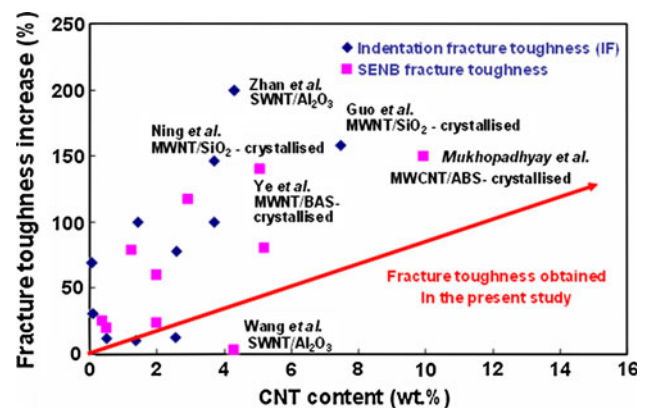


Fig. 4 Summary plot showing the relative (%) increase in fracture toughness, as measured by Vickers indentation and single edge-notched beam (SENB) methods. Volume fractions have been converted to weight fractions assuming a nanotube density of 1.65 g/cm^3 . The referenced data points are discussed in detail in the text (the full set of data is tabulated elsewhere [5]); the addition of CNT may be associated with significant microstructural variations. The continuous line represents the linear fit to the results obtained in this study (see Fig. 3)

optimistic results in the literature seem to be associated with a potentially significant change in matrix crystallinity or grain size; in these cases, it is difficult to interpret the specific contribution of the CNT addition. It should also be noted that some of the work was carried out with SWNTs and some with MWNTs. In contrast to much of the literature, the linearity of the new data, across a wide range of loading fractions, provides reasonable confidence that the observed toughening does relate directly to the CNTs, and that the dispersion quality is maintained across all samples. It is worth noting that the magnitude of the current toughening is similar to a very recent paper on a glassy aluminosilicate system, but avoids the agglomeration and property decline observed at 15 wt% MWNT in that case [24].

Toughening role of CNTs

The consequence of reducing the reinforcing fibre diameter by several orders of magnitude is not obvious and an understanding of the scaling behaviour of different toughening mechanisms is still required, particularly given the recent availability of SWNTs, MWNTs, and other nanofibres, with diameters of the order 1–100 nm. It is possible that energy dissipation during fracture propagation due to familiar mechanisms such as pull-out, crack deflection, and crack bridging may be enhanced. Indeed, these three toughening mechanisms have been suggested by many authors in CNT/ceramic composites [13, 25], but based almost always on qualitative fractography rather than quantitative analysis. In this work on model CNT/SiO₂ composites, extensive SEM characterisation has been carried out on fracture and polished surfaces after indentation tests and similar potential toughening mechanisms can be identified (Fig. 5). However, CNT collapse in “shear bands”, a toughening mechanism described in the literature [25], has not been observed in our samples. Given that the potential contribution of traditional toughening mechanisms has not often been considered quantitatively, a rather simple, classical interpretation may be informative, and is discussed further below. The validity of these equations as the fibre diameter is reduced to the nanoscale is an open question, but expectations from conventional fibre theory are a reasonable starting point. It is worth noting that the

MWNTs used in this study are relatively large and straight, and represent a good model system for exploring scaling issues. Possible additional ‘nano’ toughening mechanisms are discussed after first considering the classical theory.

In the light of experience with conventional fibre composites [26], it is likely that the nature of the interfacial bonding between the CNTs and the inorganic matrix will play an important role in the toughening response. The extent of the CNT pull-out seen on the fracture surface not only highlights the quality of the CNT dispersion in the sintered composites, but suggests an effective interaction between the CNTs and the propagating cracks. In the standard fibre theory, composite toughness is known to be maximised when the fibre length is equal to a critical value, L_c , known as the critical fibre length. L_c is the maximum fibre length for which shear failure of the interface occurs rather than tensile failure of the fibre ($L_c = r\sigma/\tau$, with τ interfacial shear stress and r fibre radius); in other words, it is the minimum length of fibre required for the stress to reach the fracture stress of the fibre [23, 26]. Classically, for short fibre composites with optimum fibre length, the fibre length pulled out at fracture will vary between 0 and $L_c/2$. In this study, the maximum and average pull-out lengths are 1.2 μm and 700 ± 200 nm (average of 100 independent nanotubes measured from SEM images), respectively, for the 15 wt% composite. From the maximum pull-out length, the critical fibre length for the current composite system is, therefore, estimated to be about 2.4 μm .

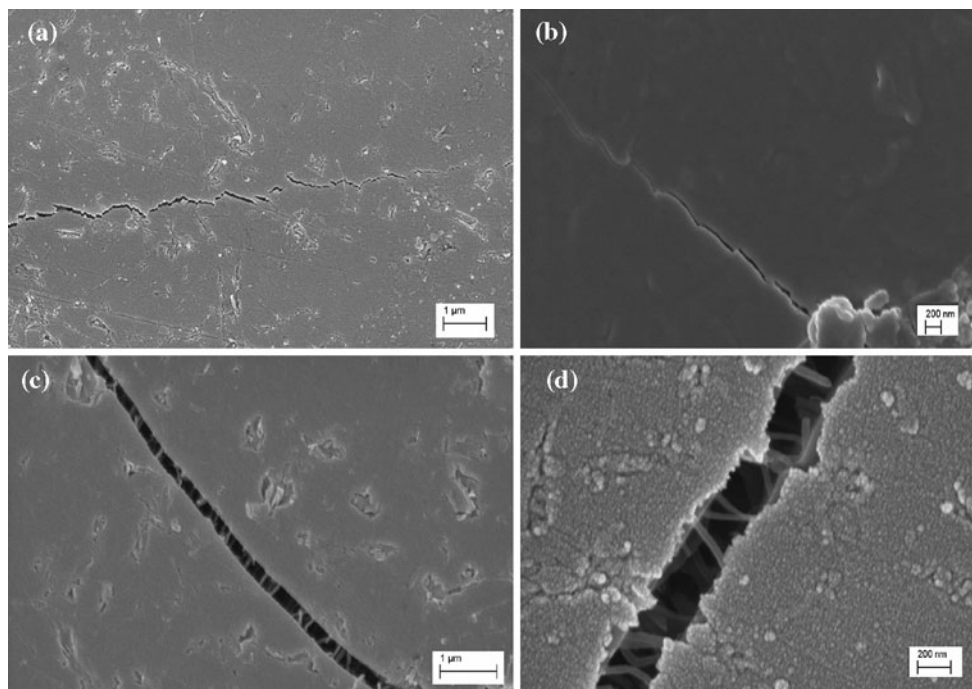


Fig. 5 SEM images showing different possible nanotube toughening mechanisms acting in the CNT/silica composites, including **a, b** crack deflection and **c, d** crack bridging

Since the actual average oxidised nanotube length ($L \approx 4.2 \mu\text{m}$), measured before consolidation, is longer than the critical length, an approximate upper estimate of the average nanotube pull-out contribution to toughening can be estimated from the following equation [26–28], by assuming that the standard, uniaxial, short fibre pull-out theory applies to the present composite system (a fraction of the fibres, given by L_c/L , will pull-out):

$$G_{\text{pull-out}} = \left(\frac{L_c}{L}\right) \frac{V_f L_c^2 \tau_i}{12r} \quad (3)$$

where V_f is the volume fraction of CNTs, L_c is the critical fibre length, τ_i is the sliding interfacial shear stress, and r is the CNT radius. Taking experimental values, $V_f = 0.19$ (15 wt%), $L_c = 2.4 \mu\text{m}$, $L = 4.2 \mu\text{m}$, and $r = 35 \text{ nm}$, together with a literature value [29, 30] $\tau_i = 10 \text{ MPa}$, an estimate for the pull-out toughening of 15 J/m^2 can be obtained. Since no direct measurements of τ_i for CNTs in glass matrices are available, the value used is based on that typically found for carbon fibre in glass matrices [30]. The very limited direct measurements that are available in polymer matrices [31] generally indeed indicate similar τ_i values for nanotubes as for conventional fibres. Further confidence is provided by considering the implied tensile strength of the nanotubes, based on the measured maximum pull-out length and assumed τ_i ; the resulting value on the order of 1 GPa, whilst at the lower end, is consistent with the range of strengths observed for CVD-grown nanotubes [32]. However, larger values of τ_i are known for carbon fibre in glass (for example, 10–35 MPa depending on glass composition) [33], and would yield commensurately higher estimated pull-out toughening and implied CNT strength figures.

Using a similar approach, an upper estimate of the energy absorbed in debonding the CNTs from the glass can be obtained from the standard expression [34] weighted by the fraction of fibres debonded:

$$G_{\text{debond}} = \left(\frac{L_c}{L}\right) \frac{2V_f L_c G_i}{r} \quad (4)$$

where G_i is the work of creating the new interface; the value for the pure glass matrix can be calculated to be $\sim 5 \text{ J/m}^2$ using the following equation:

$$G_i = \frac{(1 - \nu^2) K_{\text{IC}}^2}{E} \quad (5)$$

where ν is the Poisson's ratio [35] (~ 0.17 for silica), and K_{IC} ($0.59 \text{ MPa m}^{1/2}$, Fig. 4) and E (67 GPa) [36] are the experimental fracture toughness and modulus of elasticity of the silica monoliths, respectively. Applying this value of G_i in Eq. 4, gives an estimated debond energy $\sim 19 \text{ J/m}^2$. Alternatively, using a typical literature value [36] for the glass G_i of 3 J/m^2 , the nanocomposite debond energy is

$\sim 12 \text{ J/m}^2$. It is worth noting that both debond energy values are still expected to be overestimates since the G_i for the glass–nanotube interface will be lower than the intrinsic G_i for the glass [37]. In summary, the estimated contribution from either CNT pull-out or debonding is around 15 J/m^2 . This value can be compared to the observed toughening contribution of the nanotubes, calculated by applying Eq. 5 to the measured K_{IC} at 15 wt% CNT, and subtracting the intrinsic toughness of the glass. The resulting nanotube contribution is 16 J/m^2 , which is of the same order of magnitude as the estimated toughening mechanisms. The match is surprisingly close, given the uncertainties and assumptions involved. It does not appear that any additional toughening mechanism needs to be considered to account for the improvement observed. It is worth noting that a related, recent analysis for a MWNT/aluminosilicate glass ceramic system [24] found a similar level of toughening but attributed it to fibre bridging and debonding rather than fibre pull-out (using a version of Eq. 7, below). However, an equivalent calculation for the present system, suggests a contribution $< 1 \text{ J/m}^2$, due to the lower estimated nanotube stiffness, strength, and critical length (see above). The different mechanism may relate to localised segregation or crystallisation of the aluminosilicate glass–ceramic around the individual CNTs, leading to failure in the matrix not at the fibre surface. The resulting rough texture appeared to prevent pull-out, leading to very short ($< 50 \text{ nm}$) protruding CNT lengths and a lack of sockets, suggesting that CNT fracture predominated over the pull-out observed in Fig. 1. The matrix coating may also influence the effective fibre radius, and interfacial/tensile strengths; unfortunately, the real length of the MWCNTs, relative to the estimated debond length, was not reported in this study.

Regardless of the exact mechanism, although the CNT toughening contribution is significant for the brittle glass matrix, the absolute magnitude of the effect is obviously relatively small. Compare, for example, the fibre toughening contribution of 350 J/m^2 for 20 vol% randomly oriented short carbon fibre reinforced borosilicate glass composites [38, 39]. To understand this discrepancy in more detail, it is worth considering scaling arguments about how fibre toughening scales with fibre diameter. A simple rearrangement of the pull-out toughening equation [27, 28], assuming the fibres (strength σ_f) to be at their optimal length (L_c), gives the energy absorbed per unit area by pull-out:

$$G_{\text{pull-out}} \propto \frac{\sigma_f^2 r}{\tau_i} \quad (6)$$

Thus the pull-out toughening scales linearly with radius and, based on this simplistic model, becomes much less significant as the fibre is scaled down to the nanoscale. In this study, a multi-walled nanotube diameter ($\sim 70 \text{ nm}$) is

about 1/100th the diameter of a carbon fibre. On the other hand, it has been argued that the greater tensile strength of nanotubes will increase the toughening effects by increasing pull-out length [40]. Clearly, the strength can make a significant difference, as it is squared in Eq. 6. However, the maximum measured strength of a single highly crystalline nanotube shell (~100 GPa) [41] is about 10 times that of carbon fibre, once the central cavity of the nanotube is considered, which is insufficient to yield a net improvement of fracture toughness. In reality, the effective nanotube strength is likely to be significantly lower, due to the defects inherently present in the CVD-grown CNTs usually employed in composites, internal shear failures, or irradiation damage used to cross-link shells [41]; moreover, most high quality nanotubes have smaller diameters than mentioned here, down to around one ten thousandth of a carbon fibre diameter for single-wall nanotubes. It is worth noting that the total fibre volume that interacts with a planar crack is smaller at the nanoscale than the microscale, as the absolute pull-out length (critical length) is reduced; comparisons based on assuming equivalent volumes are only useful in constrained situations [40], such as interlaminar toughening [42, 43]. Toughness could be enhanced if the interfacial strength, τ_i , could be reduced, however, an increased nanotube length would be required to exploit this benefit. In a large number of CNT composite studies (mostly in polymer, though some in inorganic matrices), the aspect ratio of pull-out remains relatively similar to the values observed for conventional fibres (~10–100), suggesting that the ratio σ/τ is similar. Thus any benefits of increased CNT strength or reduced τ remain to be exploited. In the case of the debonding energy, the behaviour is expected to be independent of length scale, as long as the pull-out aspect ratio is constant, since the surface area generated also remains constant; however, in principle, higher nanotube strength would lead to an increasing interfacial debonding contribution, as long as the nanotube length could be optimised to match the increasing critical length (see Eq. 4). Although not reliable for the current system in which debonding toughening is similar in magnitude to the intrinsic matrix toughness, more significant debonding contributions are often correlated with the associated relaxation in strain energy in the fibres [44]. The maximum ($L = L_c$) debonding toughening can then be expressed as [26]:

$$G_{\text{debond, max}} = \frac{\sigma_f^3 r V_f}{12 \tau_i E_f} \propto \frac{\sigma_f^3 r}{\tau_i} \quad (7)$$

where E_f is the fibre modulus. Since the modulus of CNTs is essentially similar to carbon fibre (especially once the central hole is considered), the debonding toughening can be seen to scale similarly to the pull-out toughening, but with a greater strength dependence, implying scope for

improvement, associated with increased critical length, as discussed above. However, this same approach shows that the ratio of the maximum work available in pull-out and debonding is invariant with fibre dimensions and given by [44]:

$$\frac{G_{\text{pull-out, max}}}{G_{\text{debond, max}}} = 3 \frac{E_f}{\sigma_f} \quad (8)$$

Thus the contribution from the debonding, although relatively increasing with fibre strength, may not significantly compensate for lost pull-out toughening.

On the other hand, the simple models presented here are probably too pessimistic, as other factors may need to be considered at the nanoscale. For example, due to their high lateral flexibility and robustness, many CNTs are pulled-out even if not perpendicularly oriented to the crack plane (at up to 60° to the loading direction, according to one recent report [45]), leading to increased friction and deformation; some analytical calculations of the effects of nanotube curvature on toughening are just beginning to appear [46, 47]. It is worth noting that the majority of bulk, commercial, CVD-grown MWNTs have a significant degree of intrinsic curvature, although the substrate-grown CNTs used in this study are relatively straight and there is little evidence of curvature in the pulled-out segments (see Fig. 1). The use of more perfect nanotubes (with higher strengths and larger aspect ratios) with precise control of the interfacial bonding between nanotubes and matrix should significantly increase the pull-out length, raising the net toughening effects; it is worth noting that glass composition is known to have a strong effect on interfacial shear strength with carbon fibres [33], suggesting a possible means to manipulate CNT/glass composites. Additional classic toughening features such as crack bridging (Fig. 5a, b) and crack deflection (Fig. 5c, d) are also evident in the SEM images, and are prominent mechanisms in fibre reinforced ceramic composites [48]; these mechanisms may make a significant contribution to CNT composite performance if optimised in the future.

In addition to adaptations of conventional fibre toughening, it is possible that entirely new mechanisms may emerge, for example relating to the shear relaxation associated with the collapse of hollow nanotubes [25] with large internal diameters, the spring-like character of regularly coiled CNTs [49], or progressive telescopic failure of nested MWNT shells. In general, it remains an open question as to what extent the very traditional fibre composite models discussed above can be applied to nanocomposite systems, particularly as fibre diameters shrink to molecular length scales, as in the case of SWNTs. It should be noted also that detailed model calculations applying the combined micromechanical and finite element modelling, a concept suggested previously [50], may contribute to better

understanding of the quantitative effect of separate toughening mechanisms acting simultaneously.

Conclusions

A model CNT–ceramic composite system based on a dense and almost entirely amorphous silica glass matrix was used to investigate the extent of nanotube toughening in brittle materials. The particular advantage of this model system is the absence of confounding microstructural features that could affect K_{IC} , such as porosity or grain boundaries. Detailed K_{IC} measurements using both the indentation and Chevron notch tests showed that both techniques are able to provide consistent evidence of the toughening role of CNTs. Fracture toughness of the composite, as measured by both methods, increased linearly to 100–120% relative to the silica monoliths, up to unusually high CNT loadings (15 wt%). However, it was also found that the fracture toughness measured by the indentation method was overestimated by a factor of two, in the current experiments, confirming the literature reports about the difficulty of providing accurate absolute K_{IC} measurements using the indentation technique. Possible toughening mechanisms associated with CNT pull-out, CNT crack bridging, and crack deflection were identified by SEM observations, although pull-out appears to dominate. Simple quantitative estimates suggest that the conventional fibre pull-out mechanism is indeed sufficient to explain the level of toughening observed experimentally in these CNT/glass composites. For these CVD-grown CNTs, the small diameter is associated with a reduction in pull-out toughening, but a broadly constant debonding contribution, compared to conventional carbon fibre systems. However, other mechanisms may become significant in the future, for nanotubes with distinctive characteristics, such as small diameter, high strength, or unusual morphology. Further work on exploiting nanotubes for toughening brittle matrices should concentrate on identifying new mechanisms based on such features. In addition, a wide range of other functional properties remain to be studied in these, and other related, nanotube-filled inorganic matrix systems.

Acknowledgements The research carried out at IPM, Brno, Czech Republic (chevron notch fracture toughness measurement), was supported by the Czech Science Foundation under grant number 101/09/1821.

References

- Thostenson ET, Ren ZF, Chou TW (2001) *Compos Sci Technol* 61(13):1899
- Shaffer MSP, Sandler JKW (2006) In: Processing and properties of nanocomposites. World Scientific, Singapore, p 1
- Lau KT, Hui D (2002) *Compos B Eng* 33(4):263
- Harris PJ (2002) Carbon nanotubes and related structures. Cambridge University Press, Cambridge
- Cho J, Boccaccini AR, Shaffer MSP (2009) *J Mater Sci* 44(8):1934. doi:10.1007/s10853-009-3262-9
- Zhan GD, Kuntz JD, Wan JL, Mukherjee AK (2003) *Nat Mater* 2(1):38
- Wang XT, Padture NP, Tanaka H (2004) *Nat Mater* 3(8):539
- Sheldon BW, Curtin WA (2004) *Nat Mater* 3(8):505
- Jiang DT, Thomson K, Kuntz JD, Ager JW, Mukherjee AK (2007) *Scr Mater* 56(11):959
- Padture NP, Curtin WA (2008) *Scr Mater* 58(11):989
- Jiang D, Mukherjee AK (2008) *Scr Mater* 58(11):991
- Otieno G, Koos AA, Dillon F, Wallwork A, Grobert N, Todd RI (2010) *Carbon* 48(8):2212
- Ye F, Liu LM, Wang YJ, Zhou Y, Peng B, Meng QC (2006) *Scr Mater* 55(10):911
- Inam F, Yan HX, Jayaseelan DD et al (2010) *J Eur Ceram Soc* 30:153
- Inam F, Yan H, Peijs T, Reece MJ (2010) *Compos Sci Technol* 70:947
- Singh C, Shaffer M, Windle AH (2003) *Carbon* 41(2):359
- Inam F, Yan H, Reece MJ, Peijs T (2010) *Adv Appl Ceram* 109(4):240
- Anstis GR, Chantikul P, Lawn BR, Marshall DB (1981) *J Am Ceram Soc* 64(9):533
- Dlouhy I, Reinisch M, Boccaccini AR, Knott JF (1997) *Fatigue Fract Eng Mater Struct* 20:1235
- Dlouhy I, Holzmann M, Man J, Valka L (1994) *Kovove Mater Met Mater* 32(1):3
- Quinn GD, Bradt RC (2007) *J Am Ceram Soc* 90(3):673
- Ning JW, Zhang JJ, Pan YB, Guo JK (2004) *Ceram Int* 30(1):63
- Guo SQ, Sivakumar R, Kagawa Y (2007) *Adv Eng Mater* 9(1–2):84
- Mukhopadhyay A, Chu BTT, Green MLH, Todd RI (2010) *Acta Mater* 58:2685
- Xia Z, Riestler L, Curtin WA, Li H, Sheldon BW, Liang J, Chang B, Xu JM (2004) *Acta Mater* 52(4):931
- Matthews FL, Rawlings RD (2003) Composite materials: engineering and science. Woodhead Publishing Limited, Cambridge
- Fu SY, Lauke B (1997) *J Mater Sci* 32(8):1985. doi:10.1023/A:1018593931951
- Kim JK, Mai YW (1991) *Compos Sci Technol* 41(4):333
- Klug T (1994) *J Mater Sci* 29(15):4013. doi:10.1007/BF00355963
- Grande DH, Mandell JF, Hong KCC (1988) *J Mater Sci* 23(1):311. doi:10.1007/BF01174071
- Barber AH, Cohen SR, Kenig S, Wagner HD (2004) *Compos Sci Technol* 64(15):2283
- Huang YY, Knowles TPI, Terentjev EM (2009) *Adv Mater* 21:3945
- Prewo KM (1988) *J Mater Sci* 23:2745. doi:10.1007/BF00547446
- Hull D, Clyne TW (1996) An introduction to composite materials. Cambridge University Press, Cambridge
- Chawla KK (2003) Ceramic matrix composites, 2nd edn. Springer, Berlin
- Cho J, Inam F, Reece M, Rehorek L, Dlouhy I, Shaffer M, Boccaccini AR (2010) Unpublished research (paper in preparation)
- Evans AG, Zok FW (1994) *Solid State Phys* 47:177
- Sambell RAJ, Bowen DH, Briggs A, Phillips DC (1972) *J Mater Sci* 7(6):676. doi:10.1007/BF00549379
- Sambell RAJ, Phillips DC, Bowen DH (1972) *J Mater Sci* 7(6):663. doi:10.1007/BF00549378
- Wichmann MHG, Schulte K, Wagner HD (2008) *Compos Sci Technol* 68(1):329

41. Peng B, Locascio M, Zapol P, Li S, Mielke SL, Schatz GC, Espinosa HD (2008) *Nat Nanotechnol* 3:626
42. Sun LY, Gibson RF, Gordaninejad F, Suhr J (2009) *Compos Sci Technol* 69:2392
43. Blanco J, Garcia EJ, De Villoria RG, Wardle BL (2009) *J Compos Mater* 43(8):825
44. Kelly A (1970) *Proc R Soc A* 319:1536
45. Duncan RK, Chen XYG, Bult JB, Brinson LC, Schadler LS (2010) *Compos Sci Technol* 70:599
46. Chen XY, Beyerlein IJ, Brinson LC (2009) *Mech Mater* 41(3):279
47. Chen XY, Beyerlein IJ, Brinson LC (2009) *Mech Mater* 41(3):293
48. Launey ME, Ritchie RO (2009) *Adv Mater* 21(20):2103
49. Wang W, Yang K, Gaillard J, Bandaru PR, Rao AM (2008) *Adv Mater* 20:179
50. Dlouhy I, Kotoul M, Vyslouzil T, Chlup Z, Boccaccini AR (2008) *J Mater Sci* 43:4022. doi:[10.1007/s10853-007-2317-z](https://doi.org/10.1007/s10853-007-2317-z)